



## Imaging of a clickable anticancer iridium catalyst

Xiuxiu Wang<sup>a</sup>, Mingli Zhu<sup>a</sup>, Fei Gao<sup>a</sup>, Wei Wei<sup>a</sup>, Yong Qian<sup>b</sup>, Hong-Ke Liu<sup>b,\*</sup>, Jing Zhao<sup>a,\*</sup>

<sup>a</sup> State Key Laboratory of Coordination Chemistry, Institute of Chemistry and BioMedical Sciences, School of Chemistry and Chemical Engineering, Nanjing University, Nanjing 210093, China

<sup>b</sup> Jiangsu Collaborative Innovation Center of Biomedical Functional Materials, Jiangsu Key Laboratory of Biofunctional Materials, School of Chemistry and Materials Science, Nanjing Normal University, Nanjing 210023, China



### ARTICLE INFO

#### Keywords:

Iridium  
C–H activation  
Anticancer  
Imaging  
Location

### ABSTRACT

Iridium-based anticancer reagents are receiving increasing attention for their high cytotoxicity. Herein, by activating C–H bonds in the well-known antioxidant  $\alpha$ -phenyl-*N*-tert-butyl nitron (PBN), we synthesized and characterized a series of new iridium complexes. Complex 1-AMP exhibited the best antiproliferation activity towards human ovarian cancer A2780 cells. The azide group in complex 1-AMP underwent the Cu(I)-catalysed azide – alkyne cycloaddition (CuAAC) reaction and the resulting fluorescent imaging in cells suggested it mainly accumulated in mitochondria. In comparison, to eliminate cytotoxicity of Cu(I) catalyst, we conducted a reaction between complex 1-AMP and a commercialized dye via strain-promoted alkyne–azide cycloaddition (SPAAC) reaction in live cells, confirming its targeting mainly in the mitochondria. Iridium-based anticancer complexes containing a nitron ligand and azide group may offer a useful tool to probe the mechanism of metallodrugs.

### 1. Introduction

Recently considerable progress has been achieved in catalytic metallodrug development, including catalytic organoiridium (III) complex [1–3], ruthenium(II) sulfonamido ethyleneamine complexes [4], ruthenium carbene complexes [5] and ruthenium arene complexes [6]. These metal catalysts are effective in inhibiting cancer cell growth and cellular metabolic processing [7,8], especially for target-directed catalytic metallodrugs [9] through conjugation of a redox-reactive catalytic metal centre to an appropriate targeting domain [10–14]. However, in the development of catalytic metallodrugs, current challenges include insufficient rates of target inactivation [9] and cellular nucleophilic toxicity [15]. These pioneering works, contributed by Sadler, Dyson, Cowan and others, suggested that efficient targeting of metallodrugs is still essential. Representative metal complexes targeting different organelles in recent reports include photodynamic therapy agents, such as luminescent or phosphorescent iridium(III) complexes targeted to mitochondria [16,17], ruthenium(II) polypyridyl complexes targeted to lysosomes [18] and some iridium complexes targeted to autophagic lysosomes [19]. Therefore, imaging and tracking metal complexes is of crucial importance for mechanistic understanding.

However, it remains challenging to track non-fluorescent metallodrugs. The well-known. Clinical platinum drugs [20], which are generally considered to form exchange-inert complexes with genomic DNA [21,22]. Recently, DeRose et al. reported the post-treatment modification of Pt(II)

complexes, showing nuclear and intense nucleolar localization using a bioorthogonal Cu(I)-catalysed azide – alkyne cycloaddition (CuAAC) reaction in cells [23,24]. Inspired by DeRose's results, post-treatment of catalytic iridium complexes with azide modification reacted with alkyne-fluorophore via Cu(I) catalysis appears to be a promising approach for studying the mechanism and targeted location of iridium complexes.

Interestingly, fluorogenic reactions in which non- or weakly fluorescent reagents produce highly fluorescent products can be exploited to detect a broad range of compounds [25]. Click chemistry is widely used in many aspects, including nanoparticles, cell-cell interactions and protein labeling [26–28]. The common units in click chemistry include azide, alkyne and nitron. Azides are versatile reporters due to their small size and virtual absence from biological systems [29]. They can be conjugated via Staudinger ligation using modified phosphines [30], CuAAC [31,32] reaction or a strain-promoted alkyne–azide cycloaddition (SPAAC) reaction [33], which is attractive because it is rapid and does not require a potentially toxic metal catalyst. The reaction requires strained alkynes, such as difluorinated cyclooctyne (DIFO) [34], dibenzocyclooctyne (DIBO) [35,36] and bicyclononyne (BCN) [37]. Geert-Jan Boons reported fluorogenic FI-DIBO probes for visualizing biomolecules without the need for probe washout [25].

Inspired by DeRose and Geert-Jan Boons, we set out to modify our previously reported nitron-ligated organoiridium catalyst [38] with azide to probe the mechanism and targeted location of these iridium complexes.

\* Corresponding authors.

E-mail addresses: [liuhongke@nju.edu.cn](mailto:liuhongke@nju.edu.cn) (H.-K. Liu), [jingzhao@nju.edu.cn](mailto:jingzhao@nju.edu.cn) (J. Zhao).

<https://doi.org/10.1016/j.jinorgbio.2017.12.019>

Received 28 September 2017; Received in revised form 6 December 2017; Accepted 24 December 2017

Available online 29 December 2017

0162-0134/ © 2017 The Authors. Published by Elsevier Inc. This is an open access article under the CC BY-NC-ND license (<http://creativecommons.org/licenses/by-nc-nd/4.0/>).

## 2. Results and discussion

### 2.1. Synthesis of iridium-hydride complexes

Cancer cells are usually in a state of increased oxidative stress due to mitochondrial function abnormalities.  $\alpha$ -phenyl-*N*-tert-butyl nitron (PBN) can significantly inhibit the formation of reactive oxygen species (ROS) [39,40] when introduced into cells. Therefore, an organometallic hydride design combining organoiridium with a PBN group and azide unit exhibited excellent catalytic anticancer activity compared to previous research [38]. Here, we designed, synthesized, spectroscopically characterized and biologically assessed three types of iridium-hydride complexes with PBN ligands *in vitro*. Based on previous work [38], the aromatic C–H bonds in the PBN ligands were activated to generate iridium hydride complexes. We selected bidentate aryl nitron ligands based on the structure of PBN and synthesized the nitron ligand to obtain excellent yields. Next, we selected  $[\text{IrH}_2(\text{Me}_2\text{CO})_2(\text{PPh}_3)_2]\text{SbF}_6$  as the precursor organo-iridium complex, an effective catalyst in many catalytic reactions, including C–H activation to synthesize  $[\text{IrH}_2(\text{Me}_2\text{CO})_2(\text{PPh}_3)_2]\text{SbF}_6$  [38]. All of the synthesized complexes were formed via C–H activation (Scheme. S1). Finally we gained complexes **1-a**, **1-b** and **1-AMP**, which contains acetone, pyridine and 3-(azidomethyl) pyridine (AMP), respectively (Scheme. 1a). And we characterized complex **1-AMP**. yields and analytical data for the individual ligands can be found in the Supplemental Information Section.

### 2.2. Anticancer ability and iridium distribution assay

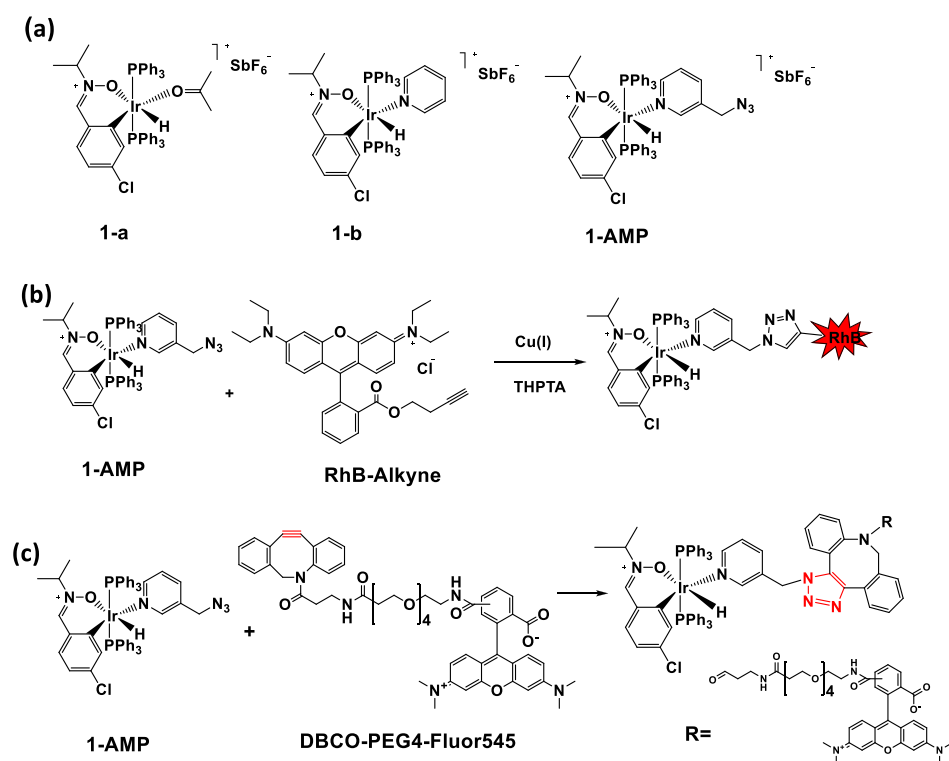
We investigated the iridium complexes **1-AMP** and other activities towards various cancer cells and their selectivity for cancer cells, with cisplatin as a positive control. We found that compound **1-AMP** has the best activity for human ovarian cancer cells ( $\text{IC}_{50} = 0.87 \mu\text{M}$ ), 19.63-fold higher than cisplatin (CDDP in Table 1). For almost all iridium complexes, the  $\text{IC}_{50}$  values were lower than that of cisplatin. The free ligand AMP and free PBN ligand **1** displayed no significant anti-proliferative activity towards cancer cells, indicating the combination of iridium with the PBN ligand; AMP was essential for anti-proliferation

(Table 1). Besides, A time course of cell proliferation with **1-AMP** treatment confirmed that complex **1-AMP** had highest toxicity especially to A2780 cells, when compared to complexes **1-a** and **1-b** (Fig. 2a and Fig. S1). Complex **1-AMP** containing isopropyl in PBN ligand and azide group showed the highest activity compared to others. For the next mechanistic experiments, **1-AMP** was selected. We found accumulated iridium complex **1-AMP** in cells, scattered in the mitochondria, nucleus and cytosome via ICP-MS with 59.4% of the complex was distributed in the mitochondria (Fig. 1b).

### 2.3. Mechanism analysis of 1-AMP in A2780 cells

Cancer cells often exhibit a disorder redox metabolism [41], and normal cells are able to control ROS levels by balancing the generation and elimination of ROS with appropriate scavenging systems [1,42]. According to the distribution of **1-AMP**, mainly in mitochondria, we examined the possible change in ROS caused by mitochondria. An increase in the ROS levels in cells after treated with **1-AMP** was observed. The ROS generation capacity of compound **1-AMP** was found to be stronger than that of  $10 \mu\text{M}$  Rosup (a reagent that can increase cellular ROS level quickly). When A2780 cells were incubated with various concentrations of **1-AMP**, MFI (Mean Fluorescence Intensity) of DCF exhibited a gradually increasing trend (Fig. S2). Besides, a comparison of ROS level in cells treated with **1-a**, **1-b** and **1-AMP** was presented in Fig. S2 and Fig. S3. These results indicated raised cellular ROS could be a possible anticancer mechanism.

Considering iridium accumulation in nuclei (Fig. 1b), and cell nuclear morphological shrinking after dealt with iridium complexes (Fig. S10), we analysed the interaction of **1-AMP** with plasmid pDNA. CD spectroscopy was performed to investigate the interaction of complex **1-AMP** with DNA. A significant increase in the intensity of the positive CD band at 262 nm suggested a strong interaction between the DNA and complex **1-AMP**. Agarose gel electrophoresis (AGE) exhibited DNA retention in sample pores when binding complex **1-AMP**, indicating a tight integration of **1-AMP** and DNA (Fig. S5). To explore the DNA damage target in mitochondria or nuclear, we selected three mitochondrial genes MTI (mitochondrially encoded NADH dehydrogenase



**Scheme 1.** (a) Chemical structure of synthesized iridium-hydride complexes with PBN ligands. (b) CuAAC reaction processing of **1-AMP** with rhodamine-alkyne. (c) SPAAC reaction process of **1-AMP** with DBCO-PET-Fluor545.

**Table 1**

IC<sub>50</sub> value of three iridium hydride complexes; **1-AMP** exhibited the best antiproliferation towards human ovarian cancer cells A2780. CDDP represents cisplatin. Ligand 1 represents free PBN ligand (chemical structure formulair is exhibited in Scheme S1).

IC <sub>50</sub> ( $\mu$ M)	A2780	A549	HeLa	H1299	HepG-2	MCF-7
1-a	11.36 $\pm$ 1.08	37.25 $\pm$ 11.67	29.42 $\pm$ 9.88	18.59 $\pm$ 2.17	33.82 $\pm$ 5.52	13.67 $\pm$ 1.79
1-b	1.84 $\pm$ 0.63	2.93 $\pm$ 0.28	1.19 $\pm$ 0.03	1.19 $\pm$ 0.55	2.31 $\pm$ 0.05	1.35 $\pm$ 0.21
1-AMP	<b>0.87 <math>\pm</math> 0.13</b>	3.03 $\pm$ 0.61	1.15 $\pm$ 0.04	1.42 $\pm$ 0.21	2.27 $\pm$ 0.12	1.32 $\pm$ 0.14
AMP	> 50	> 50	> 50	> 50	> 50	> 50
Ligand 1	> 50	> 50	> 50	> 50	> 50	> 50
CDDP	17.08 $\pm$ 3.2	22.13 $\pm$ 2.22	11.9 $\pm$ 8.25	40.58 $\pm$ 0.51	27.71 $\pm$ 2.31	17.24 $\pm$ 5.28

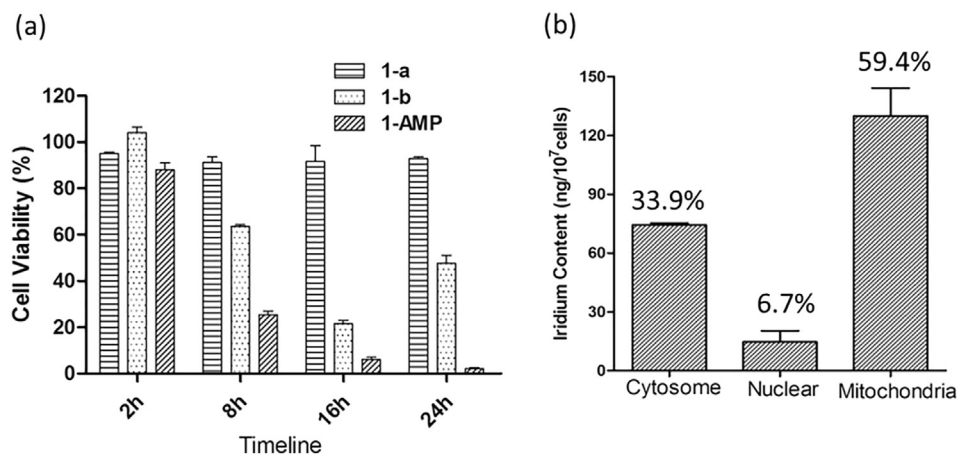


**Fig. 1.** (a) Time course of cell proliferation with 2  $\mu$ M **1-a**, **1-b** and **1-AMP** treatment in A2780 cancer cells. (b) Cellular distribution of iridium after treatment with 5  $\mu$ M **1-AMP**.

1 MT-ND1), MT2 (mitochondrially encoded ATP synthase 6 MT-ATP6), MT3 (mitochondrially encoded cytochrome *c* MT-CO2) and three nucleus genes N1 (Fragment from nuclear factor kappa B subunit 1 NFKB1), N2 (Fragment from nuclear transcription factor Y subunit alpha NFYA) and N3 (Fragment from nuclear transcription factor Y subunit beta NFYB). We compared the PCR amplifications on six gene fragments from genome in **1-AMP** treated A2780 cells and control cells (no metaldrug was added), which suggested the DNA damage was induced in nucleus when treated with complex **1-AMP**. (Fig. S7).

#### 2.4. Imaging of complex **1-AMP** in HeLa cells

A better understanding of iridium in cellular reactivity is essential to designing new and more effective therapeutics and methods of delivery. HeLa cells are always utilized as imaging model cell line for their regular cell morphology. To identify the molecular targets of Ir reagents and based on the recently reported (CuAAC) click reaction for post-treatment Pt(II) complexes in cells [24], we directly used the azide unit in **1-AMP**, and the alkyne fluorophore required for the click reaction was based on the common fluorochrome rhodamine. Encouraged by its apparent enhanced reactivity, we pursued cellular localization studies using fluorescence microscopy. We treated HeLa cells with azide-complex **1-AMP** (3  $\mu$ M, 1 h), washed, fixed and permeabilized the cells, and labelled them with the alkyne-containing rhodamine fluorophore (3  $\mu$ M, 1 h) under CuAAC conditions. This imaging result suggested iridium complexes accumulated in various target parts of cells in a very visible way. The reaction products were mainly located in mitochondria while much less was in nuclear (Fig. 2b). Importantly, the Cu-free controls showed low fluorescence from nonspecific fluorophore interactions (Fig. 2a).

However, considering possible copper toxicity to cells under the CuAAC click reaction, we instead used strain-promoted alkyne-azide cycloaddition (SPAAC). Reported tagged dibenzocyclooctyne (DBCO) can undergo fast strain-promoted cycloaddition reactions under catalyst-free conditions with azides, nitrones and nitrile oxides, as well as mono- and di-substituted diazo-derivatives [25,43] and visualized by

fluorescence microscopy. We applied this strategy in HeLa cells. First, we treated cells with complex **1-AMP** for 1 h and then added 2  $\mu$ M DBCO-PET4-Fluor545 to **1-AMP**-treated cells and untreated cells as a control at the same time. After the reaction of DBCO with the azide in **1-AMP**, we obtained an increasingly obvious fluorescent change in cells with time (Fig. 3a and b), while the control cells exhibited very weak fluorescence (Fig. 4a). We repeated this process and found significant fluorescence discrepancy of **1-AMP** treated cells with no treated HeLa cells by both whole cells fluorescence detection and flow cytometry detection methods (Fig. 3). Flow cytometry results reveal the cellular reaction fluorescence intensity was enhanced about 28 fold than probe DBCO. Cycloaddition reaction products were located in the mitochondria with much fewer observed in nuclei, confirming previous CuAAC imaging results (Fig. 4b).

Two imaging methods of the iridium complex **1-AMP** with an azide group in cells both demonstrated that it is mainly located in mitochondria, consistent with the ICP-MS data (59.4% iridium accumulation in mitochondria). These imaging results display the potential of complex **1-AMP** not only for further localization studies of iridium complexes in different cancer cell lines, but also for the ongoing goals of designing and identifying iridium-bound targets using click chemistry.

### 3. Conclusions

In summary, we have designed and synthesized a series of new iridium-hydride complexes with a PBN ligand. Complex **1-AMP** was found to exhibit the highest antiproliferative activity towards human ovarian cancer cells by inducing ROS and DNA damage. We conducted two imaging experiments based on the azide functional group in complex **1-AMP**. First, we imaged the complex **1-AMP** by CuAAC reaction with a copper catalyst. Second, a reaction without copper catalyst was performed to eliminate the possible toxicity of copper catalyst. Two imaging results for **1-AMP** confirmed that the iridium-hydride complexes are mainly concentrated in the mitochondria, consistent with the ICP-MS data. The complex **1-AMP** gathered mainly in mitochondria, which might lead to an imbalance in intracellular redox and catalytic

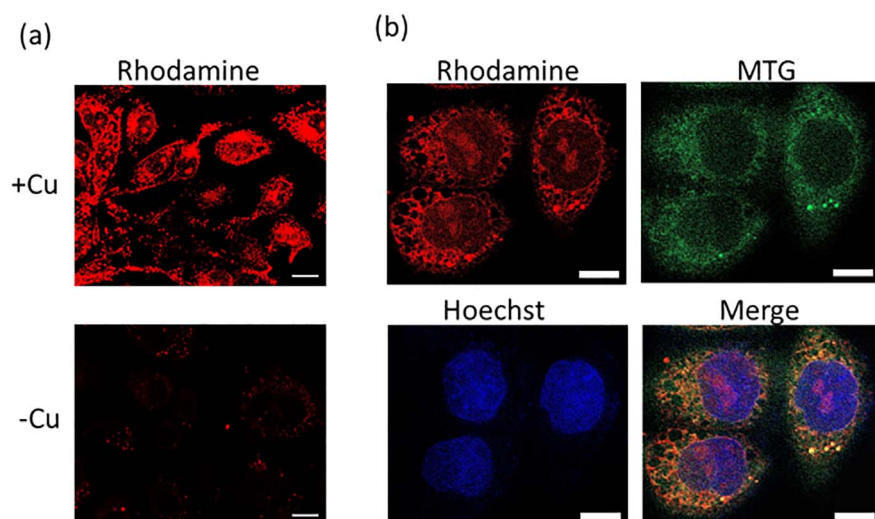


**Fig. 2.** Fluorescence image of complex **1-AMP** localization in cells via CuAAC click reaction. (a) Imaging in HeLa cells; Comparison fluorescence image of complex **1-AMP** ( $3 \mu\text{M}$ , 3 h) under CuAAC reaction condition with or without copper catalyst (+ Cu/-Cu). Scale bar:  $25 \mu\text{m}$ . (b) location of **1-AMP** in cells. MTG represents Mitochondria Tracker Green; Hoechst 33,342 represents nuclear dye. The red rhodamine fluorescence channel: excitation wavelength, 558 nm; emission collected, 575 nm. The green MTG fluorescence channel: excitation wavelength, 490 nm; emission collected, 512 nm. The blue Hoechst fluorescence channel: excitation wavelength, 353 nm; emission collected, 465 nm. Scale bar:  $10 \mu\text{m}$ .

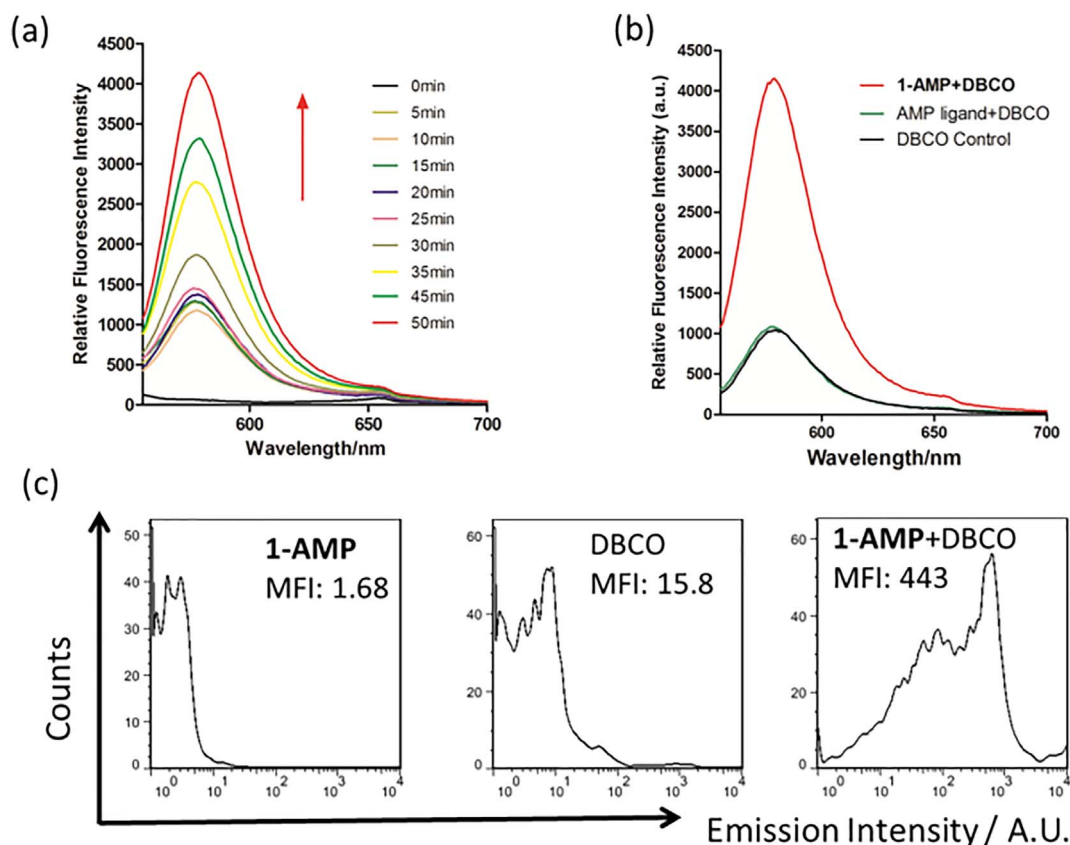


**Fig. 3.** Fluorescence detection of **1-AMP** treated cells. (a) Fluorescence change of **1-AMP** treated cells over time in 1 h, Excitation wavelength was 540 nm. (b) fluorescence intensity comparison of **1-AMP** treated cells and AMP treated cells and no treated cells as control at 50 min (right). Excitation wavelength was 540 nm. (c) Flow cytometry detecting results of **1-AMP** and AMP ligand dealt cells and no complex treated cells, excitation at 561 nm.

reaction processes resulting in cell death. Complexes with PBN ligands and azide groups may offer a general strategy to probe the mechanism of metal-based anticancer drugs.

## 4. Experimental

### 4.1. Materials and instrumentation

All solvents were of analytical reagent grade and purified according to standard Procedures [44]. Chloro(1,5-cyclooctadiene) iridium(I)

dimer was purchased from Sinocompound.  $\text{AgSbF}_6$  was purchased from Alfa Aesar. 4-Chlorobenzaldehyde, 4-(2-pyridinyl)benzaldehyde, N-isopropyl-hydroxylamine hydrochloride, 3-picoyl chloride hydrochloride, 3,3-dimethylbut-1-ene, triphenylphosphine,  $\text{Na}_2\text{SO}_4$  and  $\text{NaHCO}_3$  were purchased from Adamas. Sodium azide was purchased from Xiya Reagent. All these chemicals were used without further purification.

Nuclear magnetic resonance (NMR) spectra were acquired on Bruker 400 MHz AVANCE III for  $^1\text{H}$  NMR and  $^{13}\text{C}$  NMR at 298 K using deuterated solvents. Chemical shifts ( $\delta$ , ppm) were reported relative to

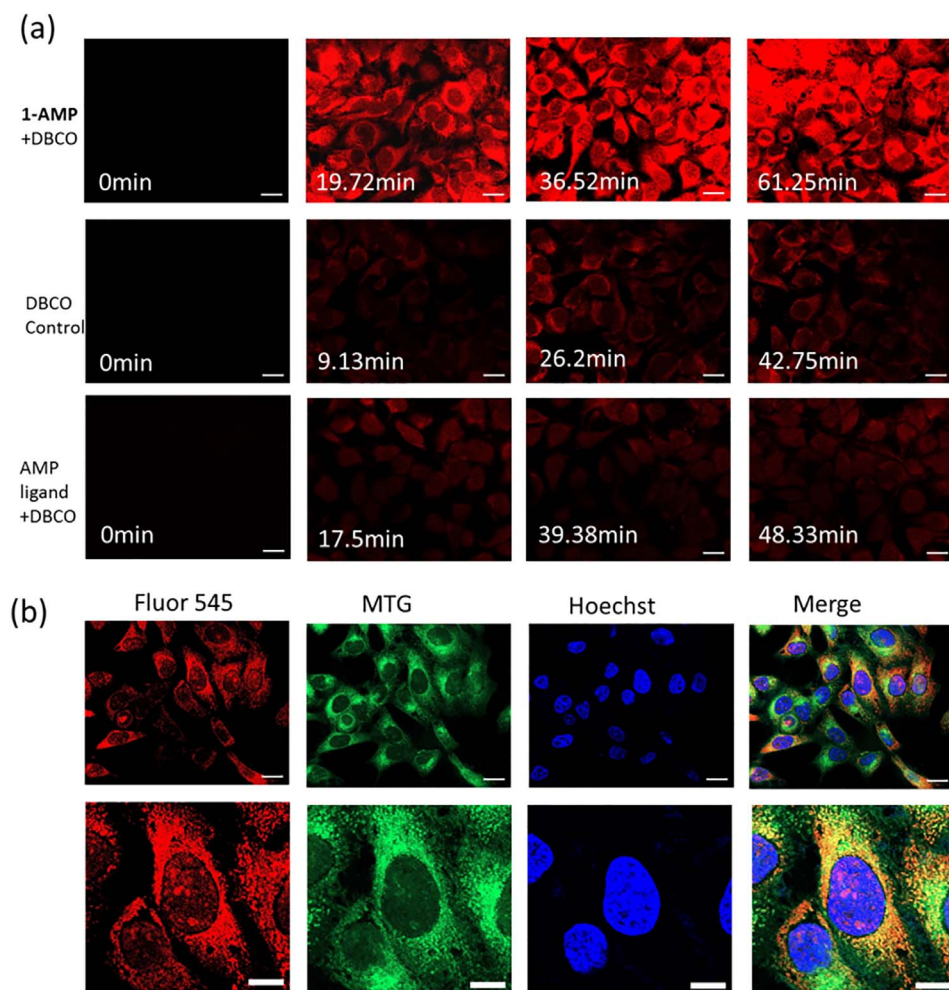


**Fig. 4.** Fluorescence image of complex **1-AMP** localization in cells via SPAAC click reaction. (a) Fluorescent processing of complex **1-AMP**-treated cells with DBCO-PET4-Fluor545 (2  $\mu$ M) shows fluorescence change over time. (b) Location in HeLa cells; Fluor545 represents reaction products fluorescence channel: excitation wavelength, 558 nm; emission collected, 575 nm. MTG represents Mitochondria Tracker Green, fluorescence channel: excitation wavelength, 490 nm; emission collected, 512 nm. The blue Hoechst fluorescence channel: excitation wavelength, 353 nm; emission collected, 465 nm. Scale bar: 25  $\mu$ m (upper), 10  $\mu$ m (lower).

tetramethylsilane (TMS) as the internal standard and the coupling constants are indicated in hertz (Hz). ESI-MS spectra were recorded on a Mariner System 5304 mass spectrometer. TLC was performed on glass-backed silica gel sheets (silica gel HG/T2354-92 GF254) and visualized under UV light (254 nm). Column chromatography was performed using silica gel (300–400 mesh).

#### 4.2. Syntheses of **1-a**, **1-b**, **1-AMP** and related ligands

##### 4.2.1. Syntheses of related ligands

(Z)-1-(4-chlorophenyl)-N-isopropylmethanimine oxide (**ligand 1**). A mixture of 4-chlorobenzaldehyde (605 mg, 4.3 mM), N-isopropylhydroxylamine hydrochloride (528 mg, 4.73 mM),  $\text{Na}_2\text{SO}_4$  (1832 mg, 12.9 mM), and  $\text{NaHCO}_3$  (1084 mg, 12.9 mM) were added to  $\text{CH}_2\text{Cl}_2$  (10 mL), and the reaction mixture was stirred and refluxed under an inert atmosphere of  $\text{N}_2$  for approximately 48 h. The resulting mixture was filtered, and the solvent was then removed under vacuum [38]. The solid was rinsed with petroleum ether, then dried in vacuum to furnish a white solid (782 mg, 92%).

3-(azidomethyl)pyridine (AMP) (**ligand 2**). To A solution of 3-Picolyl chloride hydrochloride (200 mg, 1.25 mM) and sodium azide (120 mg, 1.83 mM) in DMSO-water solvent (1,1, 2 mL) and the reaction was stirred in the air for 16 h at 50  $^\circ\text{C}$ . Sodium bicarbonate was used to quench it and the combined fractions were obtained after extraction with  $\text{CH}_2\text{Cl}_2$  (3  $\times$  10 mL). Then the organic layer was washed with water and dried by with  $\text{MgSO}_4$ , filtered and evaporated in vacuum to reveal a brown oil (82 mg, 49%).

3-Butynyl Rhodamine-B Ester (**RhB-Alkyne**). To A solution of

rhodamine-B (1.30 g, 2.70 mM) in dry  $\text{CH}_2\text{Cl}_2$  (40 mL) was added 3-butyn-1-ol (0.25 g, 3.56 mM), *N,N'*-dicyclohexylcarbodiimide (0.84 g, 4.07 mM), and 4-dimethylamino-pyridine (0.40, 0.33 mM) and the reaction was stirred in the dark for 18 h at rt. The purple reaction mixture was washed with  $\text{H}_2\text{O}$  (3  $\times$  30 mL) and the organic layer was evaporated to dryness in vacuum [45]. The purple oil was purified via flash column chromatography on silica gel ( $\text{CH}_2\text{Cl}_2$ : MeOH = 20:1). The solvent were evaporated in vacuum to reveal a purple solid (522 mg, 39%).

##### 4.2.2. Syntheses of **1-a**, **1-b** and **1-AMP**

4.2.2.1. *Synthesise of complex 1-a*. Under an argon atmosphere, a 35 mL Schlenk tube was charged with (Z)-1-(4-chlorophenyl)-N-isopropyl-methanimine oxide (32 mg, 0.15 mM), 3,3-dimethylbut-1-ene (0.7 mL),  $\text{IrH}_2(\text{PPh}_3)_2$  ( $\text{C}_3\text{H}_6\text{O}$ ) $_2\text{SbF}_6$  (145 mg, 0.14 mM), and dry acetone (3 mL). The mixture was stirred under reflux for 12 h. The solvent was removed, and the residue was washed with diethyl ether to obtain brown solid.

4.2.2.2. *Synthesise of complex 1-b*. A 25 mL Schlenk tube was charged with Complex **1-a** (200 mg, 0.17 mM), pyridine (67 mg, 0.85 mM), and dry  $\text{CH}_2\text{Cl}_2$  (2 mL). The reaction mixture was stirred and refluxed under an  $\text{N}_2$  atmosphere for approximately 12 h. Then the resulting mixture was diluted with diethyl ether, filtered and the residue was rinsed with diethyl ether to obtain brown solid.

4.2.2.3. *Synthesise of complex 1-AMP*. A 25-mL Schlenk tube was charged with complex **1-a** (145 mg, 0.12 mM), 3-(azidomethyl)

pyridine (81 mg, 0.60 mM), and dry  $\text{CH}_2\text{Cl}_2$  (2 mL). The reaction mixture was stirred and refluxed under an  $\text{N}_2$  atmosphere for approximately 12 h. The resulting mixture was diluted with diethyl ether and filtered, and the residue was rinsed with diethyl ether to obtain a yellow solid.

#### 4.3. Cancer cell growth inhibition assay

A stock solution of the new iridium complexes and cisplatin were first prepared in DMSO and then serially diluted with media to the desired test concentration. In vitro growth inhibition was performed using a CCK-8 cell proliferation and activity assay kit according to the supplier's instructions. Briefly, 5000 cells per well were seeded in 96-well plates. The cells were preincubated at 298 K in a 5%  $\text{CO}_2$  humidified atmosphere for 12 h, and supernatants were removed by suction and washed with PBS twice carefully. Then, 100  $\mu\text{L}$  of media containing different concentrations of the new Iridium (III) complexes and cisplatin were incubated for 48 h, with cisplatin assayed as a positive control. To ensure the reliability of the data, each set contained four parallel hole concentrations. Subsequently, 10  $\mu\text{L}$  CCK-8 was added to each well, and the incubation continued for an additional 3 h. The OD value was measured using an ELISA microplate reader at 450 nm. The  $\text{IC}_{50}$  (concentration of drug resulting in 50% cell growth inhibition) was calculated as the concentration of tested compound using ORIGINPRO 8 statistical software. The  $\text{IC}_{50}$  values for all of the new synthesized iridium complexes were calculated from dose-survival curves, which were obtained using a water-soluble WST-8 (2-(2-methoxy-4-nitrophenyl)-3-(4-nitrophenyl)-5-(2,4-benzene disulfonate)-2H-tetrazolium monosodium salt) assay kit (CCK-8 kit) for drug treatment.

#### 4.4. Detection of iridium accumulation of 1-AMP in cells by ICP-MS

A2780 cells were plated at a density of  $1 \times 10^6$  cells/10 mm Petri dish with 9 mL of DMEM media for 24 h. Then the cells were treated with 5  $\mu\text{M}$  Ir complex 1-AMP for 3 h. The drug-containing medium was removed, and the cells were washed with PBS for three times, trypsinized, and counted. The cytosomal, nuclear, and mitochondrial fractions were prepared using a KeyGen Mitochondria/Nuclei Isolation Kit. Collected cells were resuspended with 1.5 mL Lysis buffer, transferred to a glass homogenizer for fully grinding, then centrifuged for 5 min at 4 °C, 800 g. The precipitation was transferred to 0.5 mL Medium Buffer A upon 1 mL Medium Buffer B at 4 °C, followed by 1000 g for 10 min to get a pure nucleus precipitation. Then the nuclear part was stored in a Nuclear Store Buffer. Homogenate supernatant was then uploaded upon 0.5 mL Medium Buffer C at 4 °C, followed by 15,000 g for 10 min. After centrifugation, supernatant contained cytoplasm components and precipitation was Mitochondria. Mitochondria was then stored with Mitochondria Store Buffer. Finally iridium contents were quantified by ICP-MS analysis.

#### 4.5. Cellular ROS detection

We used the fluorescent probe 7-dichlorodihydro-fluoresce diacetate (DCFH-DA) to study the level of ROS in A2780 cells induced by compound 1-AMP. After entering cell, DCFH-DA can be hydrolyzed to DCFH and DCFH can be oxidized to fluorescent DCFH by cellular ROS. Thus, DCF content can represent cellular ROS level. 50,000 A2780 cells were seeded and incubated in 6 well plates for 24 h. Then cells were treated with 0  $\mu\text{M}$ , 5  $\mu\text{M}$ , 7.5  $\mu\text{M}$ , 10  $\mu\text{M}$  1-AMP for 1 h and 5  $\mu\text{M}$  Rosup (a reagent that can increase cellular ROS level quickly) as positive control. Then we removed the medium, adding 10  $\mu\text{M}$  DCFH-DA for 30 min in 37 °C, washing 3 times and finally collected cells for flow cytometry detection at 488 nm channel. After just 1 h of drug exposure, we observed a dramatic increase in ROS levels in cells treated with

compound 1-AMP compared to untreated cells.

#### 4.6. Cell nuclear morphological shrinking with DAPI dye

A2780 cells were cultured on a glass-bottom dish for appropriate density and treated with complex 1-AMP (2  $\mu\text{M}$ ) for 24 h, using cells without compound 1-AMP as control. Cells were washed with PBS twice, immobilized with 4% paraformaldehyde for 20 min, washed with PBS twice, incubated with DAPI dye solution for 10 min and washed with PBS twice. Then, samples were detected under fluorescence microscope (Fig. S5).

#### 4.7. Circular dichroism spectroscopy and agarose gel electrophoresis of DNA with complex 1-AMP

To solutions of PcDNA plasmid DNA (74  $\mu\text{g}/\text{mL}$ ) in sodium phosphate buffer (20 mM, pH 7.4), the appropriate complex 1-AMP was added in a total volume of 300  $\mu\text{L}$ . The mixtures were incubated for 4 h at room temperature. CD spectra were recorded on a Jasco J-815 spectropolarimeter using a quartz cuvette 385 with a path length of 1 cm with 10 accumulations per spectrum. For Agarose gel electrophoresis, 5  $\mu\text{L}$  general PcDNA plasmid DNA plasmid were taken (105  $\mu\text{g}/\text{mL}$ ) to blend with 2  $\mu\text{M}$ , 5  $\mu\text{M}$ , 10  $\mu\text{M}$  1-AMP for 4 h at room temperature using plasmid DNA as a negative control. We observed the position of the DNA using 10% agarose gel electrophoresis.

#### 4.8. PCR identification of interaction between 1-AMP and DNA in vivo

5  $\mu\text{M}$  complex 1-AMP treated A2780 cells and no complex treated cells ( $5 \times 10^7$  cells) were prepared for genome extraction using Genome Extraction Kit (KeyGen Company). Cells were washed and resuspended in 200  $\mu\text{L}$  ATL solution with 20  $\mu\text{L}$  proteinase K, incubated in 56 °C water for 60 min. Then add 200  $\mu\text{L}$  solution AL, 70 °C water for 10 min then plus 200  $\mu\text{L}$  ethanol. Then the mixture was transferred into adsorption column, 10,000 rpm for 1 min, washing the column with 500  $\mu\text{L}$  CW1 solution then 500  $\mu\text{L}$  CW2 solution, dissolved the adsorption column of DNA in  $\text{ddH}_2\text{O}$ , collecting DNA genome of 1-AMP treated cells and no complex treated cells. Then we conducted PCR amplification of six genes with 6 primers (listed in Table S2) and two genomes (1-AMP group and control group). PCR procedures were as follows: 95 °C DNA denaturation, 60 °C primers annealing and 72 °C fragment extension. Finally we observed PCR products by Agarose gel electrophoresis.

#### 4.9. Imaging of 1-AMP in HeLa cells via Cu(I)-catalysed azide – alkyne cycloaddition reaction

Human cervical cancer cell line (HeLa) cells from the American Type Culture Collection (ATCC) were cultured in DMEM media with 10% FBS at 37 °C and 5%  $\text{CO}_2$  for the appropriate density, seeded onto microscope cover slips and treated with 1-AMP complexes (5  $\mu\text{M}$ ) for 1 h. Cells were then washed with PBS twice, fixed with 4% paraformaldehyde for 20 min, permeabilized with Triton-X100 for 15 min and washed twice with 3% BSA for 10 min. The CuAAC reaction occurred with 0.5 mM  $\text{CuSO}_4$ , 5 mM THPTA, 25 mM sodium ascorbate, 100 mM phosphate buffer and 5  $\mu\text{M}$  alkyne-Rhodamine for 2 h at room temperature. Cells were washed with 3% BSA for 5 min, Triton-X100 twice for 10 min, mitochondria tracker Green MTG (From KenGEN BioTECH) (1  $\mu\text{L}$ ) for 25 min and PBS twice for 10 min. Finally, slides were incubated with one drop ProLong Diamond Antifade Reagent (Sigma) for 24 h at room temperature. A control group without Cu(I) was prepared following the same labelling protocol. Cells were observed using a Fluorescence Microscope ZEISS Axio Observer Z1 and Apointome2 software.

#### 4.10. Fluorescence detection, imaging and location of 1-AMP in HeLa cells via strain-promoted alkyne-azide cycloadditions

Human cervical cancer cell (HeLa) cells from the American Type Culture Collection (ATCC) were cultured in DMEM media with 10% FBS at 37 °C and 5% CO<sub>2</sub> for the appropriate density, seeded 5000 cells into six well plates for 24 h and treated with 1-AMP complexes (2 μM) for 1 h, AMP treated cells and no complex treated cells as control. Cells were washed with DMEM medium without phenol red (Gibco) twice and incubated with DBCO-PET4-Fluor 545 2 μM for 0 min, 5 min, 10 min, 15 min, 20 min, 25 min, 30 min, 35 min, 45 min, 50 min respectively, then wash cells with PBS twice and collected cells to underwarrant fluorescence detection in F-7000 FL Spectrophotometer.

For the fluorogenic process, we seeded 1000 cells onto microscope cover slips for 24 h, then cells underwent 2 μM 1-AMP treatment for 1 h, with AMP treated cells and no complex treated cells as the control group, incubated with DBCO-PET4-Fluor 545 for different time periods. Fluorescent change was tracked with time for 72 min, images collected at different period. Cells were observed using a Fluorescence Microscope ZEISS Axio Observer Z1 and Apotome2 software.

For location, 1000 HeLa cells were seeded onto microscope cover slips and treated with 1-AMP complexes (5 μM) for 1 h then DBCO-PET4-Fluor 545 (2 μM) for 30 min. Cells were then washed with PBS twice, fixed with 4% paraformaldehyde for 15 min. Hoechst 33,342 for 15 min and PBS twice for 10 min, then Mitochondria tracker Green MTG (From KenGEN BioTECH) (1 μL) for 25 min and PBS twice for 10 min. Cells were observed using a Fluorescence Microscope ZEISS Axio Observer Z1 and Apotome2 software.

#### Abbreviations

DMSO	dimethylsulfoxide
PBS	phosphate buffered saline
ROS	reactive oxygen species
IC <sub>50</sub>	the concentration at which half of the cells remains viable
DMEM	Dulbecco's modified eagle medium
DCFH	2',7'-dichlorofluorescein
CM-DCFH-DA	5(6)-chloromethyl-2',7'-dichlorodihydrofluorescein diacetate
FBS	Fetal Bovine Serum
PCR	Polymerase Chain Reaction
CCK-8	Cell counting kit-8
CuAAC	Cu(I)-catalysed azide – alkyne cycloaddition
SPAAC	strain-promoted alkyne-azide cycloaddition
DFAAC	difluorinated cyclooctyne
DIBO	dibenzocyclooctyne
BCN	bicyclononyne
DBCO	dibenzocyclooctyne
PEG	polyethylene glycol
Fluor545	Fluorescence group with excitation wavelength at 545 nm
DBCO-PEG4-Fluor545	dibenzocyclooctyne-polyethylene glycol 4-Fluor545
MFI	Mean Fluorescence Intensity

#### Acknowledgements

Financial support was provided by the National Science Foundation of China (21622103, 21571098 and 21671099), the Natural Science Foundation of Jiangsu Province (BK20160022), the Key International (Regional) Joint Research Program (Grant No. 21420102002), the Jiangsu Higher Education Institutions [Priority Academic Program Development (PAPD)], “Summit of the Six Top Talents” Program, Grant 247450).

#### Appendix A. Supplementary data

Supplementary data to this article can be found online at <https://doi.org/10.1016/j.jinorgbio.2017.12.019>.

#### References

- [1] Z. Liu, I. Romero-Canelon, B. Qamar, J.M. Hearn, A. Habtemariam, N.P.E. Barry, A.M. Pizarro, G.J. Clarkson, P.J. Sadler, *Angew. Chem. Int. Ed.* 53 (2014) 3941–3946.
- [2] Z. Liu, R.J. Deeth, J.S. Butler, A. Habtemariam, M.E. Newton, P.J. Sadler, *Angew. Chem. Int. Ed.* 52 (2013) 4194–4197.
- [3] Z. Liu, A. Habtemariam, A.M. Pizarro, S.A. Fletcher, A. Kisova, O. Vrana, L. Salassa, P.C.A. Bruijninx, G.J. Clarkson, V. Brabec, P.J. Sadler, *J. Med. Chem.* 54 (2011) 3011–3026.
- [4] J.J. Soldevila-Barreda, I. Romero-Canelon, A. Habtemariam, P.J. Sadler, *Nat. Commun.* 6 (2015) 6582.
- [5] P. Schwab, R.H. Grubbs, J.W. Ziller, *J. Am. Chem. Soc.* 118 (1996) 100–110.
- [6] S. Hashiguchi, A. Fujii, K.J. Haack, K. Matsumura, T. Ikariya, R. Noyori, *Angew. Chem. Int. Ed.* 36 (1997) 288–290.
- [7] C.G. Hartinger, P.J. Dyson, *Chem. Soc. Rev.* 38 (2009) 391–401.
- [8] C.G. Hartinger, N. Metzler-Nolte, P.J. Dyson, *Organometallics* 31 (2012) 5677–5685.
- [9] J.C. Joyner, J.A. Cowan, *Braz. J. Med. Biol. Res.* 46 (2013) 465–485.
- [10] L. Hocharoen, J.A. Cowan, *Chem-Eur. J.* 15 (2009) 8670–8676.
- [11] S. Bradford, J.A. Cowan, *Chem. Commun.* 48 (2012) 3118–3120.
- [12] J.C. Joyner, L. Hocharoen, J.A. Cowan, *J. Am. Chem. Soc.* 134 (2012) 3396–3410.
- [13] J.C. Joyner, J.A. Cowan, *J. Am. Chem. Soc.* 133 (2011) 9912–9922.
- [14] N.H. Gokhale, J.A. Cowan, *J. Biol. Inorg. Chem.* 11 (2006) 937–947.
- [15] R.H. Crabtree, *Chem. Rev.* 115 (2015) 127–150.
- [16] Y. Chen, W.C. Xu, J.R. Zuo, L.N. Ji, H. Chao, *J. Mater. Chem. B* 3 (2015) 3306–3314.
- [17] K.Q. Qiu, H.Y. Huang, B.Y. Liu, Y.K. Liu, P.Y. Zhang, Y. Chen, L.N. Ji, H. Chao, *J. Mater. Chem. B* 3 (2015) 6690–6697.
- [18] H. Huang, B. Yu, P. Zhang, J. Huang, Y. Chen, G. Gasser, L. Ji, H. Chao, *Angew. Chem. Int. Ed.* 54 (2015) 14049–14052.
- [19] L. He, C.P. Tan, R.R. Ye, Y.Z. Zhao, Y.H. Liu, Q. Zhao, L.N. Ji, Z.W. Mao, *Angew. Chem. Int. Ed.* 53 (2014) 12137–12141.
- [20] B. Rosenberg, L. Vancamp, T. Krigas, *Nature* 205 (1965) (698 – +).
- [21] F. Arnesano, M. Losacco, G. Natile, *Eur. J. Inorg. Chem.* (2013) 2701–2711.
- [22] E.R. Jamieson, S.J. Lippard, *Chem. Rev.* 99 (1999) 2467–2498.
- [23] H.C. Kolb, M.G. Finn, K.B. Sharpless, *Angew. Chem. Int. Ed.* 40 (2001) (2004 – +).
- [24] R. Wirth, J.D. White, A.D. Moghaddam, A.L. Ginzburg, L.N. Zakharov, M.M. Haley, V.J. DeRose, *J. Am. Chem. Soc.* 137 (2015) 15169–15175.
- [25] F. Friscourt, C.J. Fahrni, G.J. Boons, *Chemistry* 21 (2015) 13996–14001.
- [26] P. Shi, E.G. Ju, Z.Q. Yan, N. Gao, J.S. Wang, J.W. Hou, Y. Zhang, J.S. Ren, X.G. Qu, *Nat. Commun.* 7 (2016) 13088–13097.
- [27] Y.J. Song, K.G. Qu, C. Xu, J.S. Ren, X.G. Qu, *Chem. Commun.* 46 (2010) 6572–6574.
- [28] K. Lang, J.W. Chin, *ACS Chem. Biol.* 9 (2014) 16–20.
- [29] M.F. Debets, C.W.J. van der Doelen, F.P.J.T. Rutjes, F.L. van Delft, *ChemBioChem* 11 (2010) 1168–1184.
- [30] C.I. Schilling, N. Jung, M. Biskup, U. Schepers, S. Brase, *Chem. Soc. Rev.* 40 (2011) 4840–4871.
- [31] M. Meldal, C.W. Tornøe, *Chem. Rev.* 108 (2008) 2952–3015.
- [32] D.C. Kennedy, C.S. McKay, M.C.B. Legault, D.C. Danielson, J.A. Blake, A.F. Pegoraro, A. Stolow, Z. Mester, J.P. Pezacki, *J. Am. Chem. Soc.* 133 (2011) 17993–18001.
- [33] J.C. Jewett, C.R. Bertozzi, *Chem. Soc. Rev.* 39 (2010) 1272–1279.
- [34] J.A. Codelli, J.M. Baskin, N.J. Agard, C.R. Bertozzi, *J. Am. Chem. Soc.* 130 (2008) 11486–11493.
- [35] F. Friscourt, C.J. Fahrni, G.J. Boons, *J. Am. Chem. Soc.* 134 (2012) 18809–18815.
- [36] F. Friscourt, P.A. Ledin, N.E. Mbua, H.R. Flanagan-Steet, M.A. Wolfert, R. Steet, G.J. Boons, *J. Am. Chem. Soc.* 134 (2012) 5381–5389.
- [37] J. Dommerholt, S. Schmidt, R. Temming, L.J.A. Hendriks, F.P.J.T. Rutjes, J.C.M. van Hest, D.J. Lefeber, P. Friedl, F.L. van Delft, *Angew. Chem. Int. Ed.* 49 (2010) 9422–9425.
- [38] X. Song, Y. Qian, R. Ben, X. Lu, H.L. Zhu, H. Chao, J. Zhao, *J. Med. Chem.* 56 (2013) 6531–6535.
- [39] R.A. Floyd, Y. Kotake, K. Hensley, D. Nakae, Y. Konishi, *Mol. Cell. Biochem.* 234 (2002) 195–203.
- [40] R.A. Floyd, H.C.C.F. Neto, G.A. Zimmerman, K. Hensley, R.A. Towner, *Free Radic. Biol. Med.* 62 (2013) 145–156.
- [41] D. Trachootham, J. Alexandre, P. Huang, *Nat. Rev. Drug Discov.* 8 (2009) 579–591.
- [42] R.A. Cairns, I.S. Harris, T.W. Mak, *Nat. Rev. Cancer* 11 (2011) 85–95.
- [43] A.R. Sherratt, M. Chigrinova, D.A. MacKenzie, N.K. Rastogi, M.T.M. Ouattara, A.T. Pezacki, J.P. Pezacki, *Bioconjug. Chem.* 27 (2016) 1222–1226.
- [44] P.M. Schwab, C. Moosmann, K. Dopf, H.J. Eisler, *Opt. Express* 23 (2015) 26533–26543.
- [45] R. Wirth, J.D. White, A.D. Moghaddam, A.L. Ginzburg, L.N. Zakharov, M.M. Haley, V.J. DeRose, *J. Am. Chem. Soc.* 137 (2015) 15169–15175.